Laminar Flow Past Three Closely Spaced Monodisperse Spheres or Nonevaporating Drops

R. S. Ramachandran,* T.-Y. Wang,† C. Kleinstreuer,‡ and H. Chiang†
North Carolina State University, Raleigh, North Carolina 27695

A basic understanding of the highly nonlinear interaction effects of multiple, closely spaced spheres or droplets on the fluid flow patterns and fluid mechanics parameters is of importance for the improved design of a variety of fluid-particle systems. Streamlines, vorticity contours, flow separation angles, and individual drag/interaction coefficients are presented for steady laminar axisymmetric flow past a linear array of three spheres or droplets. A finite element method has been used to solve the complete Navier-Stokes equations for the system parameter ranges of $1 \leq Re_d \leq 200$ (particle Reynolds numbers) and $2 \leq d_{ij} \leq 6$ (dimensionless particle spacings). The verified computer simulation results indicate that the separation angles and effective drag coefficients of interacting spheres deviate significantly from solitary spheres at all Reynolds numbers. The differences between solid spheres and nonevaporating water drops in air with stress-induced internal circulation are only marginal.

Nomenclature

$a_{1,2,3}$ = constants
$b_{1,2,3}$ = constants
C_{Ds} = total drag coefficient of single sphere
$C_{D,k}$ = total drag coefficient of sphere k
C_p = form drag coefficient
d,D = sphere/droplet diameter
d_{ij} = intersphere distances
f = function
L = representative droplet spacing
$\overline{Nu}$ = average Nusselt number
p = pressure
Pr = Prandtl number
r = radial cylindrical coordinate
R_0 = radius of sphere
Re = Reynolds number
U_0 = characteristic or freestream velocity
u,v = velocity components
V = magnitude of two-dimensional droplet velocity
v = velocity vector
$\forall$ = variable
z = axial coordinate

Greek Symbols

α = drag coefficient ratio
$\hat{\delta}$ = unit vector
ν = kinematic viscosity
ρ = density
θ = spherical coordinate
$\Delta\theta$ = difference in separation angles ($\Delta\theta_{sep} = \theta_{sep} - \theta_{sep,s}$)
θ_{sep} = separation angle measured from forward stagnation point
ψ = stream function
τ = tangential stress
ζ = vorticity function
σ = normal stress
γ = surface tension

Subscripts

D = total drag
d = based on diameter
g = gas phase
i = index for particle spacing ($i = 1,2$)
j = index for particle spacing ($j = i + 1$)
k = index for particle identification ($k = 1,2,3$)
ℓ = liquid phase
s = single sphere
sep = flow separation
∞ = at infinity

Superscript

* = dimensional quantities

Introduction

A BASIC understanding of steady laminar flow past multiple spheres or drops is important for design applications where noncollisional interaction effects are significant. Examples include spray systems, particle suspension flows, fluidized beds, and spherical structures in a linear array. Of interest in this paper are the flow patterns around three spheres and the spheres' flow separation angle and drag coefficients in the Reynolds number range of $1 \leq Re_d \leq 200$ at different spacings; the effect of slip at the interface of drops on fluid flow parameters has also been investigated.

While single-sphere analyses are now well documented,[1,2] multiple-sphere studies are restricted to two-sphere/droplet systems.[3-5] Zaprynov and Toshov[4] solved the Navier-Stokes equations and the energy equation numerically for steady laminar flow past two spheres in tandem for $Re_d \leq 40$, as Tal et al.[3] had done using bispherical coordinates. Raju and Sirignano[5] employed a finite-difference code[6] with mesh generator[7] to solve the unsteady Navier-Stokes equations ($Re_d \leq 100$) for two vaporizing droplets in tandem. They again confirmed earlier observations that (close) particle spacings affect fluid flow parameters as well as heat and mass transfer rates. Mulholland et al.[8] measured two-dimensional trajectories of a stream of monodisperse nonevaporating droplets in the initial Reynolds number range of $90 \leq Re_d \leq 290$. Then they curve-fitted a simple trajectory model to the experimental data to obtain an effective drag coefficient as a function of the Reynolds number and a droplet spacing representative of the entire droplet streamer. Earlier contributions are based on the classical paper by Stimson and Jefferey,[9] who used bispherical coordinates to solve for the stream function considering

Received June 28, 1989; revision received Feb. 23, 1990.

*Research Associate.
†Research Assistant.
‡Associate Professor, Department of Mechanical and Aerospace Engineering.

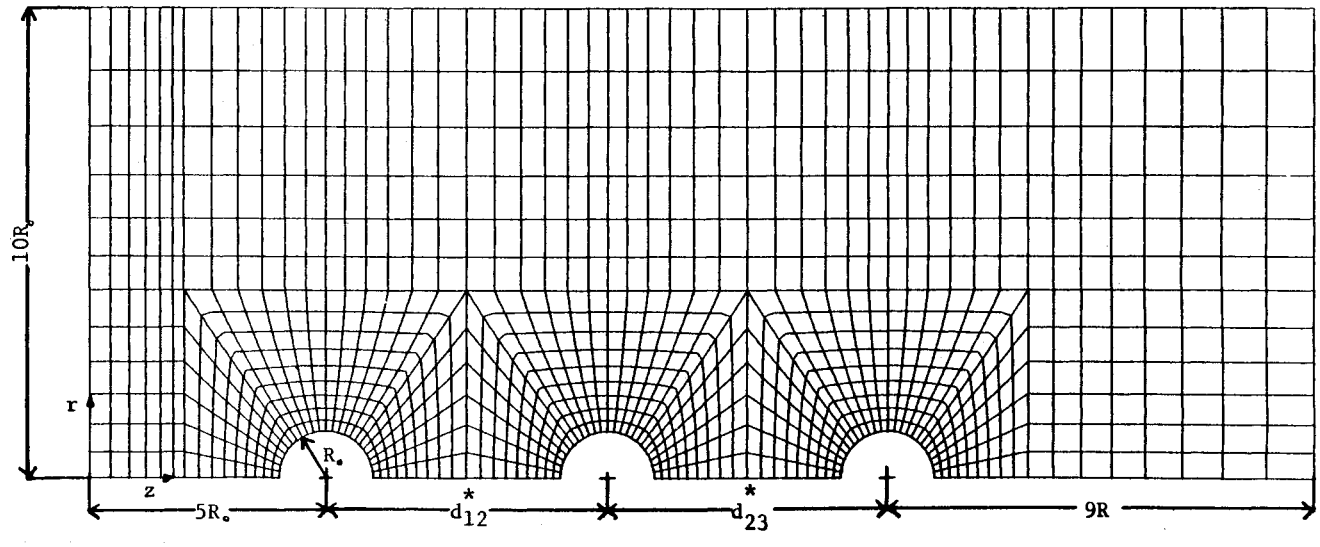

Fig. 1 Representative axisymmetric quadrilateral finite element mesh and coordinate system for linear array of spheres or droplets.

axisymmetric, low Reynolds number flow past two spheres. They derived a correction factor representing interaction effects for Stokes' drag formula. Their analysis was extended to the case of two slowly moving drops by Wacholder and Weihs.[10] Assuming axisymmetric potential flow ($Re \to \infty$), Bentwich and Miloh[11] obtained an analytic solution for two spheres in tandem. Relevant experimental work is limited to flow visualization and measurements of the drag coefficients and the flow separation angles of two-sphere systems.[12,13]

For the analysis of interaction effects of spheres and droplets in a linear array or on a one-dimensional trajectory, it is necessary to consider more than two spheres or droplets; however, three to five particles should be sufficient.[14] Hence, we concentrate on three spheres, or three droplets with shear-induced internal circulation aligned with the freestream. The complete momentum equation has been solved for steady laminar axisymmetric incompressible flow using a finite element method. It is assumed that steady (attached) wakes exist in the Reynolds number range of interest.[15]

Analysis

A representative finite element mesh and the axisymmetric (cylindrical) coordinate system for the computational domain are depicted in Fig. 1. With the stated assumptions, the nondimensional equations and associated boundary conditions are

Continuity equation:

$$\nabla \cdot v_{g,\ell} = 0 \tag{1}$$

Momentum equation:

$$(v_{g,\ell} \cdot \nabla)v = -\nabla p + (1/Re_{d,\ell})\nabla^2 v_{g,\ell} \tag{2}$$

where the velocity vector and the del-operator have two components each. In the gas phase axisymmetric cylindrical coordinates $v_r = v_g$, $v_z = u_g$ and $\nabla = \hat{\delta}_r(\partial/\partial r) + \hat{\delta}_z(\partial/\partial z)$ are used; whereas in the liquid phase (droplets), axisymmetric spherical coordinates, $v_R = v_\ell$, $v_\theta = u_\ell$ and $\nabla = \hat{\delta}_R(\partial/\partial R) + \delta_\theta(1/R)(\partial/\partial\theta)$ are used.

Boundary conditions:

1) At inlet and upper domain boundary

$$u_g = 1 \qquad \text{and } v_g = 0 \tag{3a}$$

2) Along centerline

$$v_g = 0 \qquad \text{and } \partial v_g/\partial r = 0 \tag{3b}$$

3) At the solid-gas interfaces (three spheres)

$$v_{g,\ell} = 0 \tag{3c}$$

and for the liquid-gas interfaces (three droplets)

$$v_g = v_\ell;\ \tau_g = \tau_\ell \qquad \text{and } (p - \sigma)\Big|_g = \left[p - \sigma - \frac{4\gamma}{d}\right]_\ell \tag{3d}$$

4) At the domain outlet

$$v_g = 0 \qquad \text{and } \partial u_g/\partial z = 0 \tag{3e}$$

The dimensionless variables are defined as

$$u_{g,\ell} = \frac{u^*_{g,\ell}}{U_0}, \quad v_{g,\ell} = \frac{v^*_{g,\ell}}{U_0}, \quad p = \frac{p^*}{\rho U_0^2}, \quad \text{and } Re_{d,\ell} = \frac{U_0 d}{\nu}$$

Numerical Method

The governing equations [Eqs. (1) and (2)] subject to the conditions of Eqs. (3a–e) are solved using a widely accepted finite element software package.[16] Actually, the penalty function approach is used where the continuity requirement is weakened by replacing Eq. (1) with $\nabla \cdot v_g = \epsilon p$. The penalty parameter is very small, i.e., $\epsilon = \mathcal{O}(10^{-6})$. The elements chosen are isoparametric quadrilaterals with nine nodes and biquadratic velocity and linear pressure approximations.[17] A

Table 1 Comparison of characteristic flow parameters for sphere(s)

Single sphere Re_d	Separate angle θ_{sep}		Drag coefficient C_{Ds}	
	Reference[18]	Present results	Reference[19]	Present results
10	—	—	4.24	4.40
20	—	—	2.61	2.71
40	144.0	144.4	1.82	1.83
50	139.3	139.5	1.63	1.65
100	126.5	125.1	1.186	1.187
200	116.4	116.5	0.916	0.916

Two spheres $Re_d = 40$	Drag coefficients $C_{D,k}$; $k = 1,2$					
	$d_{12} = 1.5$		$d_{12} = 2$		$d_{12} = 4$	
	$C_{D,1}$	$C_{D,2}$	$C_{D,1}$	$C_{D,2}$	$C_{D,1}$	$C_{D,2}$
Reference[12]	0.80	0.54	—	—	—	—
Reference[3]	0.88	0.53	—	—	—	—
Reference[4]	—	—	0.88	0.621	0.92	0.74
Present results	0.84	0.56	0.88	0.624	0.94	0.73

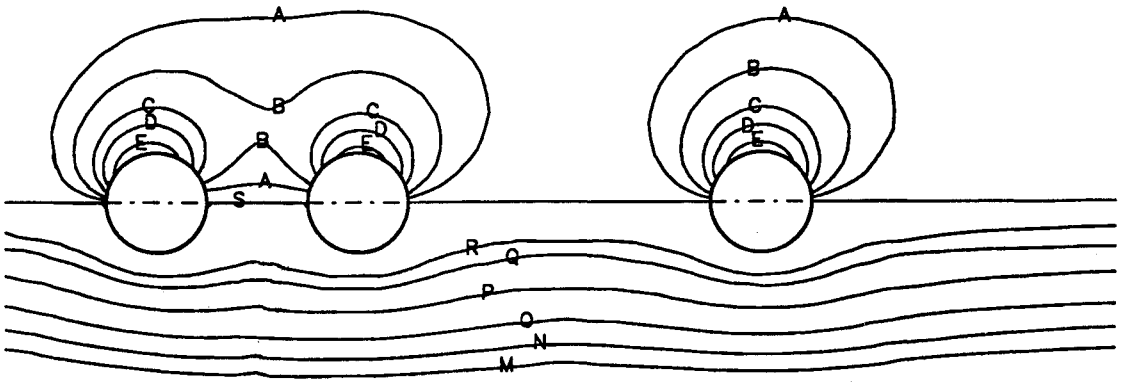

Fig. 2a Vorticity contours and streamlines for three spheres at $\overline{d_{12}} = 2$ and $d_{23} = 4$, ($Re_d = 1$).

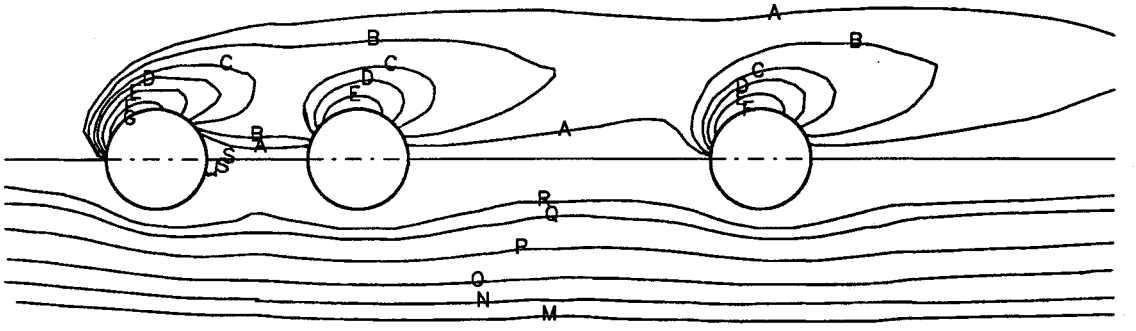

Fig. 2b Vorticity contours and streamlines for three spheres at $\overline{d_{12}} = 2$ and $d_{23} = 4$, ($Re_d = 20$).

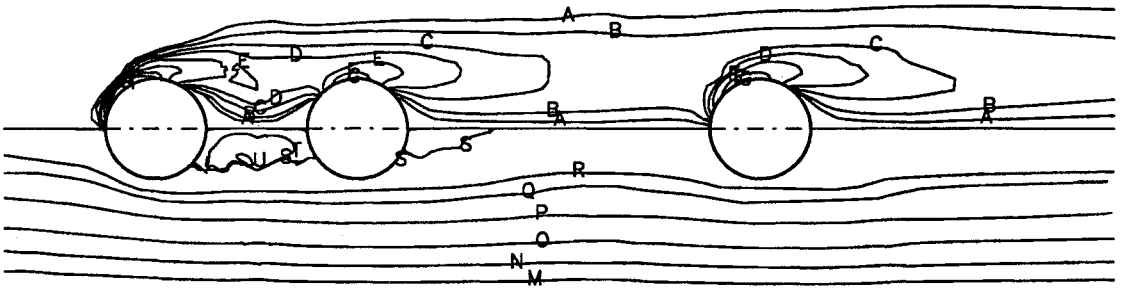

Fig. 2c Vorticity contours and streamlines for three spheres at $\overline{d_{12}} = 2$ and $d_{23} = 4$, ($Re_d = 100$).

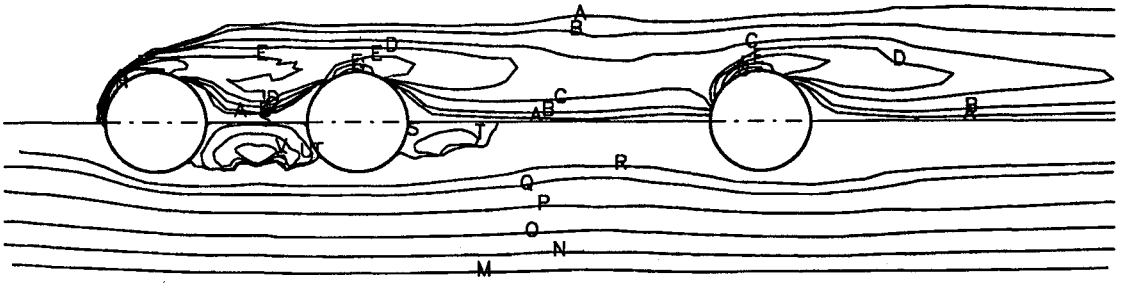

Fig. 2d Vorticity contours and streamlines for three spheres at $\overline{d_{12}} = 2$ and $d_{23} = 4$, ($Re_d = 200$).

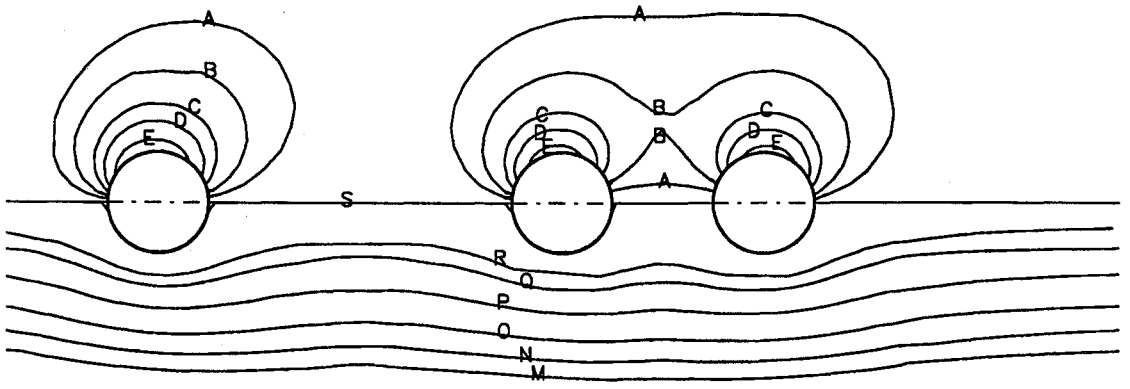

Fig. 3a Vorticity contours and streamlines for three spheres at $\overline{d_{12}} = 4$ and $d_{23} = 2$ ($Re_d = 1$).

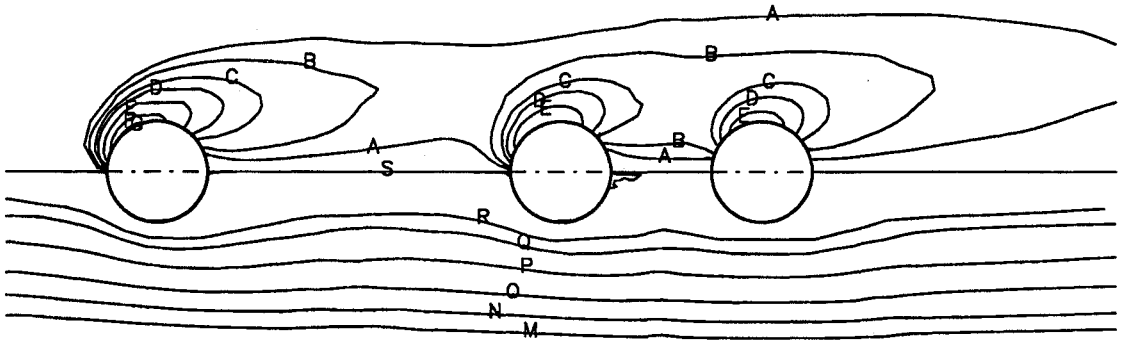

Fig. 3b Vorticity contours and streamlines for three spheres at $\overline{d_{12}} = 4$ and $d_{23} = 2$ ($Re_d = 20$).

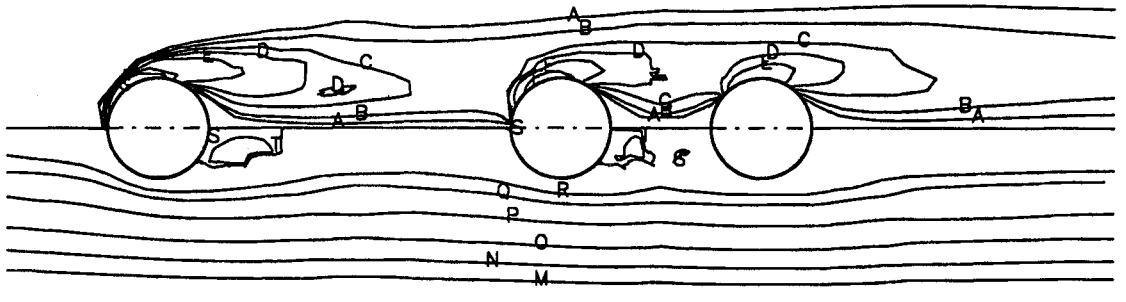

Fig. 3c Vorticity contours and streamlines for three spheres at $\overline{d_{12}} = 4$ and $d_{23} = 2$ ($Re_d = 100$).

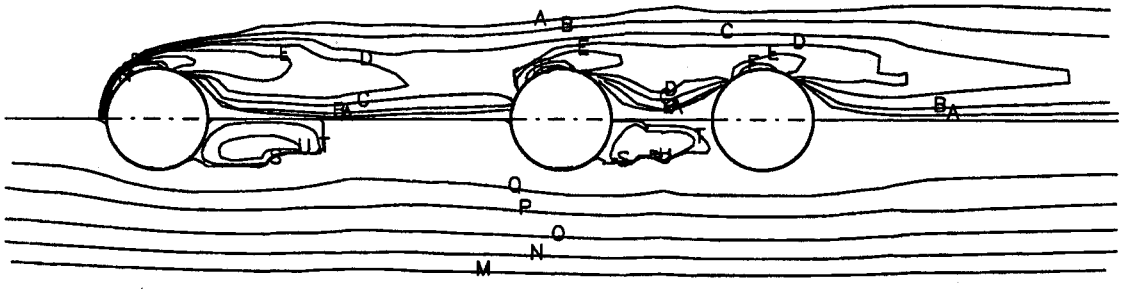

Fig. 3d Vorticity contours and streamlines for three spheres at $\overline{d_{12}} = 4$ and $d_{23} = 2$ ($Re_d = 200$).

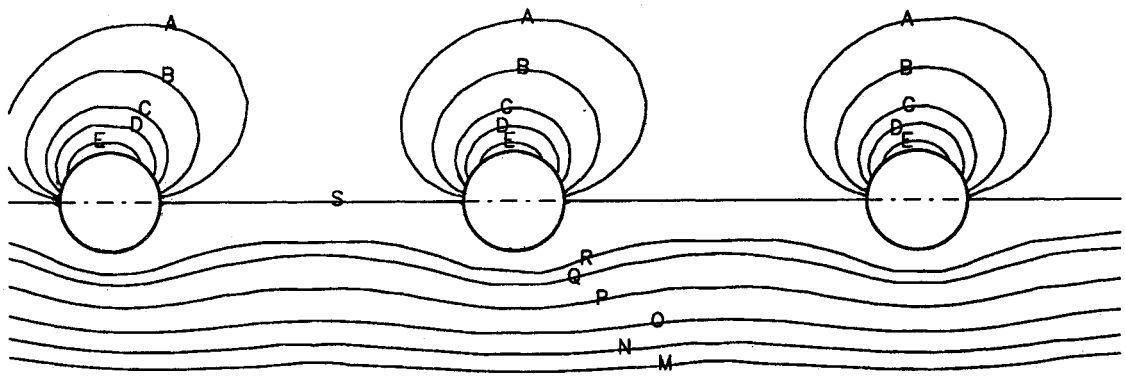

Fig. 4a Vorticity contours and streamlines for three spheres at $\overline{d_{12}} = d_{23} = 4$ ($Re_d = 1$).

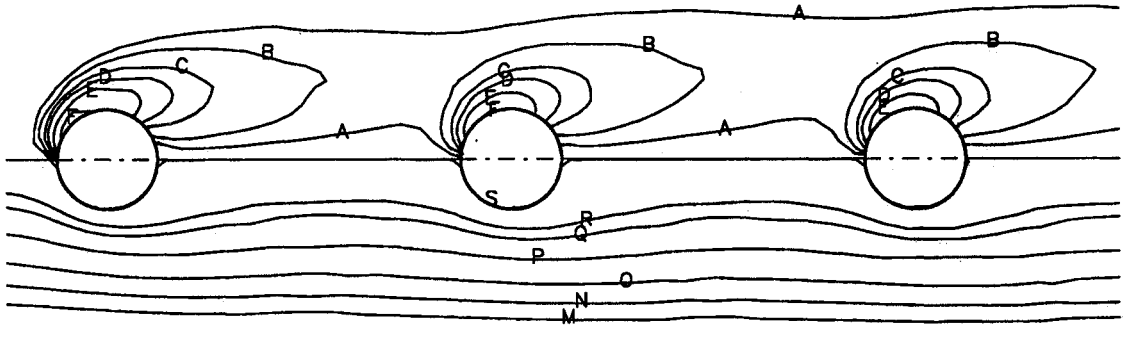

Fig. 4b Vorticity contours and streamlines for three spheres at $\overline{d_{12}} = d_{23} = 4$ ($Re_d = 20$).

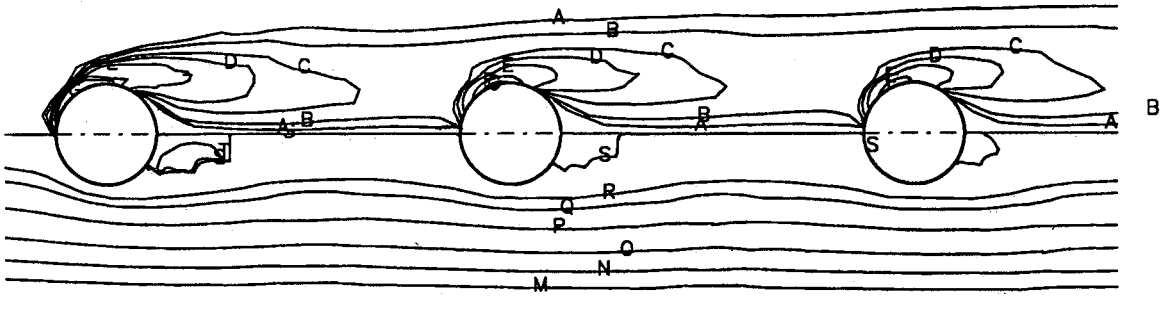

Fig. 4c Vorticity contours and streamlines for three spheres at $\overline{d_{12}} = d_{23} = 4$ ($Re_d = 100$).

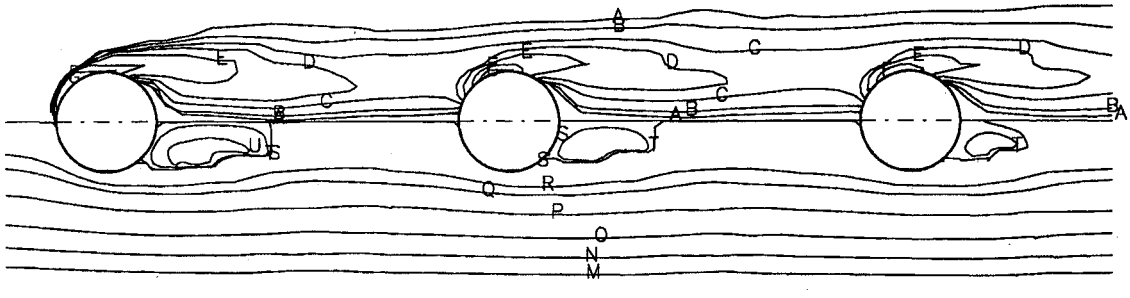

Fig. 4d Vorticity contours and streamlines for three spheres at $\overline{d_{12}} = d_{23} = 4$ ($Re_d = 200$).

quasi-Newton algorithm is used for solving the nonlinear equations with a reformation of the Jacobian matrix every five steps. In order to facilitate convergence, a slower but more robust successive substitution method is applied for the first three steps to bring the solution within the radius of convergence of the quasi-Newton method. Subsequently, the faster convering quasi-Newton scheme is invoked. Convergence was achieved when the error criterion $\epsilon = |(\forall^{new} - \forall^{old})/\forall^{new}| \leq 10^{-5}$ was fulfilled. A typical computer run required 6 hr of central processing unit (CPU) time on an IBM 4341.

A mesh of variable density is required for cost-effective computer runs. Very small elements are placed at the interface and large elements near the domain boundaries. A smooth transition from fine to coarse mesh regions has been provided. The overall mesh size has been obtained in accordance with the boundary conditions of Eqs. (3a) and (3e) by trial and error. In order to avoid overlapping lines, the mesh shown in Fig. 1 does not contain several layers of finite elements along the spherical interface. Independence of the simulation results from the mesh density has been successfully tested based on repeat calculations with finer meshes.

With the given postprocessing capabilities, stress calculations, velocity vector graphs, as well as plots of streamlines, vorticity contours and pressure profiles can be conveniently executed.

Results and Discussion

The numerical code has been verified with published data sets for single-sphere and two-sphere systems (Table 1). The empirical correlations for the single-sphere separation angle $\theta_{sep} = \theta(\tau = 0)$ and the total drag coefficient C_{Ds} are given in Clift et al.[18] and White,[19] respectively.

Table 2 Parameter variations for three-sphere case

$Re_d = U_0 d/\nu$:	= 1, 20, 50, 100 and 200
$d_{ij} = d^*_{ij}/d$:	= 2, 4 and 6

Table 3 Letter values for vorticity contours and streamlines (cf. Figs. 2 to 4)

Vorticity contour plots	A = 0.25;	B = 0.50; C = 1.00;	D = 1.50;	E = 2.50
	F = 5.00;	G = 7.50; H = 10.0;	I = 15.0;	J = 20.0
Streamline plots	M = 1.00;	N = 0.75; O = 0.50;	P = 0.25;	Q = 0.10
	R = 0.05;	S = 0.00; T = −0.001;	U = −0.005;	V = −0.01

$$\theta_{sep,s} = 180 - 42.5\,[\ell n\,(Re_d/20)]^{0.483} \quad \text{for } 20 < Re_d < 400 \quad (4)$$

$$C_{Ds} = \frac{24}{Re_d} + \frac{6}{1+\sqrt{Re_d}} + 0.4 \quad \text{for } 1 < Re_d < 2 \times 10^5 \quad (5)$$

Measured data points for two spheres in tandem were published by Rowe and Henwood,[12] and theoretical solutions were obtained by Tal et al.[3] and Zaprynov and Toshov.[4]

For a linear array of three spheres or droplets, the freestream Reynolds number ($1 \leq Re_d \leq 200$) and the intersphere distances ($1 \leq d_{ij} \leq 6$) between the first and second sphere and between the second and third sphere have been varied (Table 2). The flow separation angles as well as the streamlines and vorticity contours for representative combinations of these parameters are shown in Figs. 2–4. A wealth

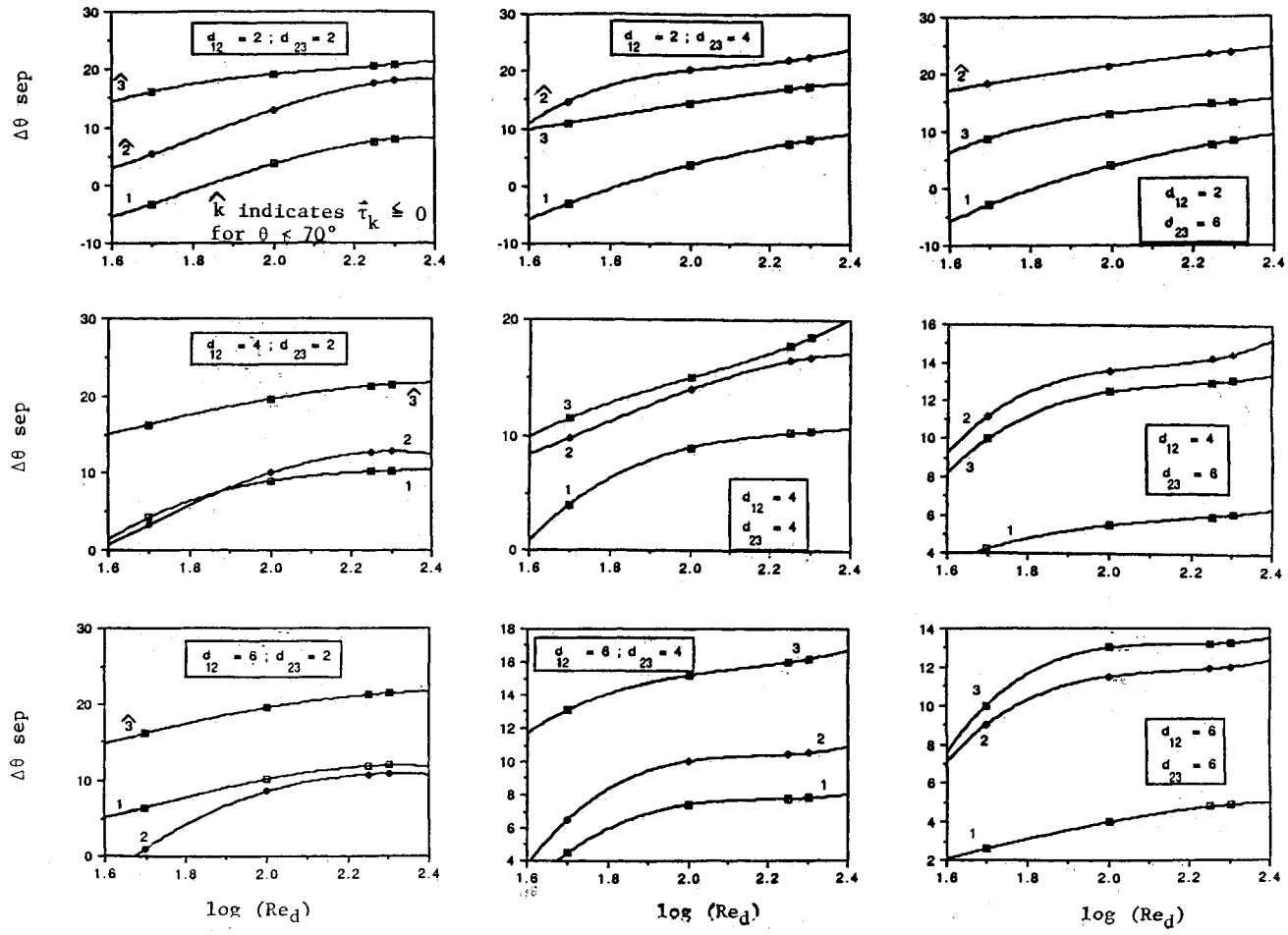

Fig. 5 Deviation in flow separation angles of interacting spheres from solitary spheres for different Reynolds numbers and sphere distances ($\Delta\theta_{sep} = \theta_{sep} - \theta_{sep,s}$).

Table 4 Effects of slip at the spherical interface on fluid flow parameters ($Re_d = 200$, $d_{ij} = 4$)

	Spheres			Droplets		
	$C_{D,p}/C_D$	C_D	$\theta_{sep}\|_{\tau=0}$	$C_{D,p}/C_D$	C_D	$\theta_{sep}\|_{\tau=0}$
Particle[1]	0.516	0.432	124.0 deg	0.515	0.421	125.8 deg
Particle[2]	0.545	0.417	130.4 deg	0.553	0.412	132.2 deg
Particle[3]	0.545	0.375	132.1 deg	0.556	0.369	133.1 deg

of data has been produced for all combinations of Re, d_{12} and d_{23} within the given ranges, and new correlations for $C_{D,k} = C_{D,k}(Re, d_{ij})$ have been developed (see Fig. 6). In summary, at almost all Reynolds numbers and intersphere distances, the deviations of θ_{sep} and C_D from single sphere values are significant. Convection heat transfer results in terms of flowfield isotherms and average Nusselt number correlations for each interacting sphere $\overline{Nu}_k = \overline{Nu}_k(Re, Pr, d_{ij})$ are presented in a complementary paper.[20]

Flow Patterns

Fluid flow patterns for steady laminar axisymmetric flow past three spheres are depicted in Figs. 2a–4d in terms of vorticity contours (upper half) and streamlines (lower half). The magnitudes of the dimensionless vorticity function (ζ = const) and stream function (ψ = const) are given in Table 3 where $A < B < C \ldots < J$ for vorticity contours and $M > N > 0 \ldots > V$ for streamlines.

The vorticity contour plots show clearly: 1) the boundary-layer effect with increasing freestream Reynolds numbers, 2) the "body-pairing" of (two) closely spaced spheres (see Figs. 2a–3d vs Figs. 4a and 4b), 3) the convection effect for $Re_d > 1$, and 4) the downstream extent of the wakes for $Re_d > 20$. The streamlines depict the onset and size of the near-wakes as a function of the Reynolds number and intersphere distances. Delayed flow attachment at the front of the second sphere at $Re_d = 100$ and 200 is indicated in Figs. 2c and 2d, and this reappears for the third sphere for the arrangement given in Figs. 3c and 3d. This phenomenon, due to particle interaction, is further discussed in the next section.

Separation Angles

The flow separation angles for spheres 2 and 3 are always larger than those for a single sphere (Fig, 5) where θ_{sep} is measured from the forward stagnation point. Earlier flow separation on the first sphere can be expected when the second sphere is relatively close ($d_{12} \leq 2$) and the Reynolds number is low ($20 \leq Re \leq 60$) as shown in Fig. 5 and indicated in Fig. 2b. When the distance between any two spheres is small ($d_{ij} \approx 2$) and $Re > 50$, two "points" of zero wall shear stress appear on the second or back sphere; one point is due to the near-wake recirculation causing delayed flow attachment on the front part of the closely spaced sphere and the second point representing the final flow separation (see Fig. 5). The recirculation zone between two closely spaced spheres in a linear three-sphere array is wider for the front pair (see Figs. 2b–2d) than for the back pair (see Figs. 3b–3d). Both zones increase in width when the Reynolds number increases. Upstream effects are clearly demonstrated when comparing $\Delta\theta(Re_d)$ of the first sphere at $d_{12} = d_{23} = 2$ with the $\Delta\theta$ values at $d_{12} = d_{23} = 6$. Strong interaction effects appear also in the sequence of graphs in Fig. 5 where d_{23} is fixed at $d_{23} = 2$ and d_{12} is varied, i.e., $2 \leq d_{12} \leq 6$. In this case, as d_{12} is increased, $\Delta\theta$ for sphere 1 increases from separation angles less than θ_{sep} for a single sphere, when $Re_d \leq 60$ and $d_{12} = 2$, to separation angles exceeding those of the second sphere when $Re_d \leq 200$ and $d_{12} = 6$. For very small d_{23} spacings, it is conceivable that spheres 2 and 3 behave almost like a single body. Such a body-pair behavior is evident when the flow patterns in Figs. 2a–2d and 3a–3d are compared with those in Figs. 4a–4d.

Total Drag Coefficients

Reliable C_D-correlations are most desirable for the analysis and design of multiple sphere systems. For a single sphere, the drag coefficient C_{Ds} is a function of the Reynolds number only. It can be expected from the flow patterns, separation angles, and interaction effects discussed in the previous sec-

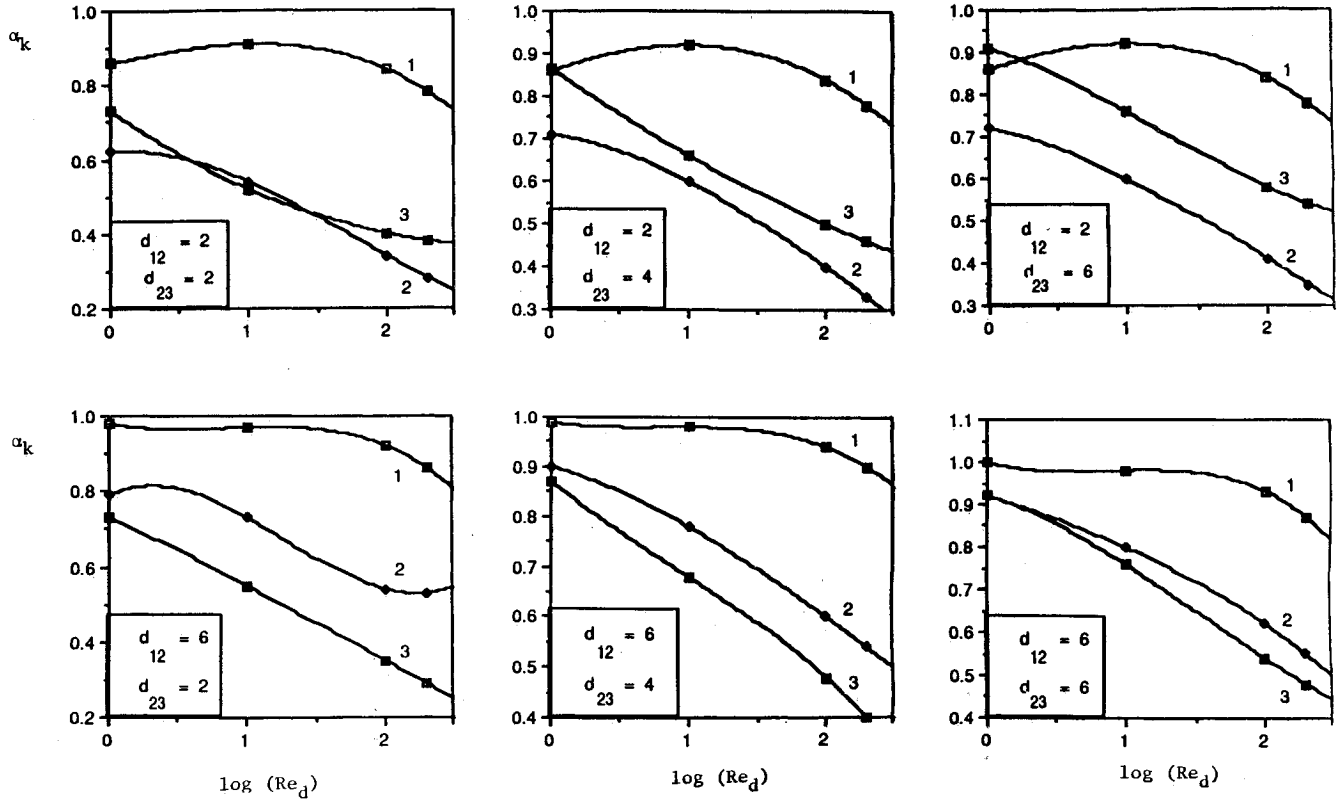

Fig. 6 Ratio of drag coefficients for individual spheres as a function of Reynolds number and intersphere distance ($\alpha_k \equiv C_{D,k}/C_{Ds}$).

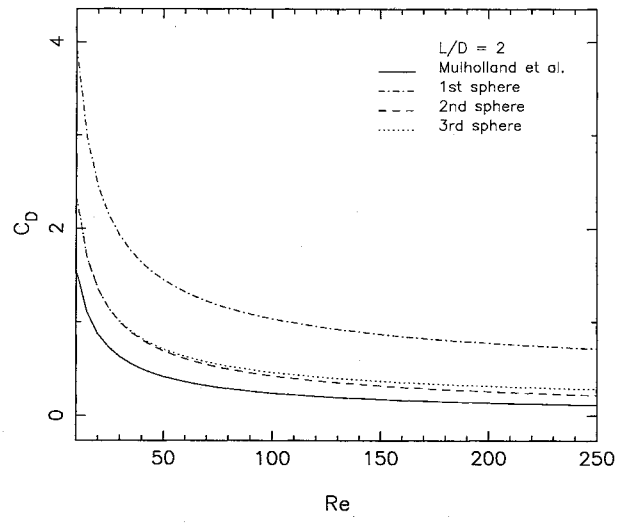

Fig. 7a Comparison of individual drag coefficients of closely spaced spheres with a representative drag coefficient for a droplet streamer[8] ($L/D = 2$).

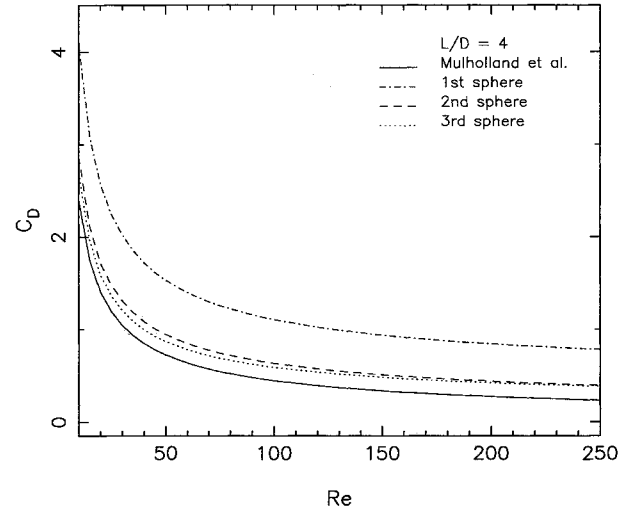

Fig. 7b Comparison of individual drag coefficients of closely spaced spheres with a representative drag coefficient for a droplet streamer[8] ($L/D = 4$).

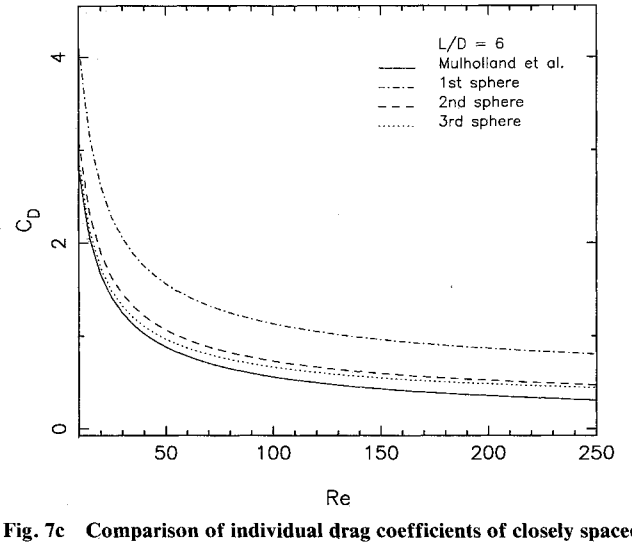

Fig. 7c Comparison of individual drag coefficients of closely spaced spheres with a representative drag coefficient for a droplet streamer[9] ($L/D = 6$).

tions for three spheres, that

$$\alpha_k \equiv \frac{C_{D,k}}{C_{Ds}} = \frac{f_1(Re_d; d_{12}, d_{23})}{f_2(Re_d)} = f_3(Re_d, d_{12}, d_{23}); \quad k = 1,2,3 \qquad (6)$$

Considering that the interaction effects are highly nonlinear and their influence causes drag reduction, when compared with a single sphere, α_k should have the following functional form:

$$\alpha_k = 1 - b_1 Re_d^{a_1}\left(\frac{b_2}{d_{12}^{a_2}} + \frac{b_3}{d_{23}^{a_3}}\right); \qquad k = 1,2,3 \qquad (7)$$

where $a_1 - a_3$ and $b_1 - b_3$ are constants for each sphere and $\lim \alpha_k \to 1$ when $d_{ij} \to \infty$. Results from a curve-fitting procedure indicated that Eq. (7) is most appropriate for the second sphere, i.e., $k = 2$. In order to obtain better agreements with sphere-1 and sphere-3 data bases, generated from computer experiments, postulates for α_1 and α_3 differed somewhat from Eq. (7). Using a least-squares analysis, the following expressions for α_k have been developed.

First sphere:

$$\alpha_1 = 1 - 0.096\, Re_d^{0.2475} d_{12}^{-0.965} e^{0.4764/d_{23}} \qquad (8)$$

Second sphere:

$$\alpha_2 = 1 - Re_d^{0.1593}(0.2932/d_{12}^{0.4876} + 0.1341/d_{23}^{0.4242}) \qquad (9)$$

Third sphere:

$$\alpha_3 = 1 - 0.325\,(\ell n\, Re_d + 1)^{0.603} e^{-0.282/d_{12}} d_{23}^{-0.385} \qquad (10)$$

The average curve-fitting errors, i.e., the deviations of $C_{D,k}$ in Eqs. (8-10) from the computer generated values, range from 2.4% ($k = 1$) to 4.7% ($k = 3$). Maximum errors are always less than 9% and may occur at low Reynolds numbers ($Re_d < 20$). As $d_{12} \to \infty$, α_1 approaches one, as to be expected. Similarly, as $d_{23} \to \infty$, α_3 approaches one. However, the correlation for α_2 retains the influence of the third sphere when $d_{12} \to \infty$ and remains affected by the first sphere when $d_{23} \to \infty$.

The drag coefficient ratios for each affected sphere, i.e., α_k [log (Re_d)] with the intersphere distance d_{ij} as a parameter, are plotted in Fig. 6. It is evident that the interaction characteristics of a multiple-sphere system are more pronounced at high Reynolds numbers, i.e., α_k ($k = 2,3$) decreases when Re_d increases. The ratio α_1 depends almost exclusively on the distance d_{12}. As d_{12} increases, α_1 reaches unity asymptotically and that limit for d_{12} where $\alpha_1 \approx 1$ increases with increasing Reynolds number. Similar observations hold for spheres 2 and 3 when they become isolated.

Nonevaporating Droplets

When the three solid spheres are replaced by droplets where the internal-to-external fluid viscosity ratio is high, the interfacial shear stress induces a weak liquid-phase circulation (e.g., for water drops in an airstream, $|v_{\ell,\max}| = 0.03\, U_0$ for $Re_d = 200$), which causes a small delay in flow separation and reduces the total drag coefficient. For example, the C_D- and θ_{sep}-values for water drops in an isothermal airstream with $Re = 200$ and $d_{ij} = 4$ are given in Table 4.

Figures 7a-c show a comparison between the individual drag/interaction coefficients $C_D(Re_d)$ of Eqs. (8-10) with $d_{12} = d_{23} \equiv L/D$ as a parameter and the curve-fitted drag coefficient[8] representative of spherical droplets on a two-dimensional trajectory. Mulholland et al.[8] defined the lumped-parameter distance between any two droplets as $L = L_0\, V(t)/v_0$ where $V(t) = (u^2 + v^2)^{1/2}$ and u, v are the velocity components in the x and y direction. In general, the "measured" $C_D(Re)$ curve is being approached with increasing particle spacing and

with higher particle number. Discrepancies between the individual graphs remain because of two-dimensional effects lumped by Mulholland et al.[8] into the definition of $C_D F_D/[(\rho/2)\ V^2]$, upstream or elliptic effects apparent in Fig. 7a when compared to Fig. 7c, and of course experimental as well as computational errors.

Conclusions

Laminar axisymmetric flow past a linear array of three spheres or drops is a representative system for investigating downstream/upstream interaction effects present in one-dimensional multiparticle arrangements. The analysis can be used in a variety of fluid-particle models. Applications include high density sprays, particle suspension flows, fluidized beds, and fluid flow/spherical structure systems. The Navier-Stokes equations describing laminar incompressible axisymmetric flow have been numerically solved to study flow patterns (ψ and ζ contours) and to calculate fluid mechanics parameters (θ_{sep} and C_D) for interacting spheres or droplets at $2 \le d_{ij} \le 6$ and $1 \le Re_d \le 200$. Vortex shedding, which may occur when $Re_d = \mathcal{O}(100)$, has not been considered.

As can be expected, interaction effects on the flow parameters are highly nonlinear, and their impact increases with decreasing intersphere spacing and increasing Reynolds numbers. A sphere with two neighbors is most strongly affected, and downstream interaction effects usually override upstream effects at high Reynolds numbers. The flow separation angles for spheres 2 and 3 are always larger than θ_{sep} for a single sphere. A relatively smaller θ_{sep} for the first sphere, i.e., a wider near-wake, can be seen when $d_{12} \le 2$ and $Re_d < 60$. Delayed flow attachment has been observed on the front part of the second sphere in any close two-sphere arrangement ($d_{ij} \approx 2$ and $Re_d > 50$). Such "particle pairs" behave almost as a single body.

Expressions for the drag coefficients of the individual spheres $C_{D,k}/C_{Ds} = 1 - f(Re_d, d_{ij})$ have been developed. They should be most useful for the modeling, analysis, and design of certain fluid-particle systems. Liquid spheres with weak internal droplet circulations (e.g., water drops in air) differ only marginally from solid spheres.

Acknowledgment

This work has been supported in part by the Department of Energy, Office of Basic Energy Science Grant DE-FG05-87ER13728.

References

[1]Conner, J. M., and Elghobashi, S. E., "Numerical Solution of Laminar Flow Past a Sphere with Surface Mass Transfer," *Numerical Heat Transfer,* Vol. 12, 1987, pp. 57-82.

[2]Finlayson, B. A., and Olson, J. W., "Heat Transfer to Spheres at Low to Intermediate Reynolds Numbers," *Chemical Engineering Communications,* Vol. 58, 1987, pp. 431-447.

[3]Tal, R., Lee, D. N., and Sirignano, W. A., "Heat and Momentum Transfer Around a Pair of Spheres in Viscous Flow," *International Journal of Heat and Mass Transfer,* Vol. 27, No. 11, 1984, pp. 1953-1962.

[4]Zaprynov, Z. D., and Toshov, E. T., "Hydrodynamics and Heat Transfer around Two Separated Spherical Particles," *Proceedings of the Eighth International Conference on Heat Transfer,* ASME, New York, Vol. 5, 1986, pp. 2549-2553.

[5]Raju, M. S., and Sirignano, W. A., "Unsteady Navier-Stokes Solution for Two Interacting Vaporizing Droplets," AIAA Paper, Jan. 1987.

[6]Dwyer, H. A., and Sanders, B. R., "Detailed Combustion of Unsteady Droplet Dynamics," *Twentieth Symposium on Combustion,* Combustion Institute, Pittsburgh, PA, 1984.

[7]Thompson, J. F., Thames, F. C., and Mastin, C. W., "TOMCAT-A Code for Numerical Generation of Boundary-Fitted Curvilinear Coordinate Systems on Fields Containing Any Number of Arbitrary Two-Dimensional Bodies," *Journal of Computational Physics,* Vol. 24, 1977, pp. 274-302.

[8]Mulholland, J. A., Srivastava, R. K., and Wendt, J. O. L., "Influence of Droplet Spacing on Drag Coefficient in Nonevaporating, Monodisperse Streams," *AIAA Journal,* Vol. 26, No. 10, 1988, pp. 1231-1237.

[9]Stimson, M., and Jefferey, G. B., "The Motion of Two Spheres in a Viscous Fluid," *Proceedings of the Royal Society of London,* Ser. A, Vol. III, 1929, pp. 110-116.

[10]Wacholder, E., and Weihs, D., "Slow Motion of a Fluid Sphere in the Vicinity of Another Sphere or a Plane Boundary," *Chemical Engineering Science,* Vol. 27, 1972, pp. 1817-1828.

[11]Bentwich, M., and Miloh, T., "On the Exact Solution for the Two Sphere Problem in Axisymmetric Potential Flow," *Journal of Applied Mechanics,* Vol. 45, 1978, pp. 463-468.

[12]Rowe, P. N., and Henwood, G. A., "Drag Forces in a Hydraulic Model of a Fluidized Bed-Part I," *Transactions Institute of Chemical Engineers,* Vol. 39, 1961, pp. 43-56.

[13]Tsuji, Y., Morikawa, Y., and Terashima, K., "Fluid-Dynamic Interaction Between Two Spheres," *International Journal of Multiphase Flow,* Vol. 8, 1982, pp. 71-82.

[14]Ramachandran, R. S., Kleinstreuer, C., and Altwicker, E. R., "Mass Transfer to an Accelerating Multidrop System," *International Journal of Heat and Mass Transfer,* Vol. 30, No. 3, 1987, pp. 607-612.

[15]Nakamura, I., "Steady Wake Behind a Sphere," *Physics of Fluids,* Vol. 19, No. 1, 1976, pp. 5-8.

[16]Engelman, M. S., "FIDAP-A Fluid Dynamics Analysis Package," *Advanced Engineering Software,* Vol. 4, 1982, pp. 163-166.

[17]Cuvelier, C., Segal, A., and Van Steenhoven, A. A., *Finite Element Methods and Navier-Stokes Equations,* D. Reidel, Dordrecht, Holland, 1986.

[18]Clift, R., Grace, J. R., and Weber, M. E., *Bubbles, Drops and Particles,* Academic, New York, 1978.

[19]White, F. M., *Viscous Fluid Flow,* McGraw-Hill, New York, 1974.

[20]Ramachandran, R. S., Kleinstreuer, C., and Wang, T.-Y., "Forced Convection Heat Transfer of Interacting Spheres or Droplets," *Numerical Heat Transfer,* Vol. 15, Pt. A, 1989, pp. 471-487.